1 Liquid Ar scintillation from neutron induced recoils

C. Amsler, W. Creus, A. Ferella, C. Regenfus, and J. Rochet

Weakly Interacting Massive Particles (WIMPs) are prime candidates for dark matter. The interaction of WIMPs in scintillators (e.g. noble liquids such as liquid argon, LAr) leads to nuclear recoils generating scintillation light. Unfortunately, the light signal from highly ionizing particles is heavily quenched and detection thresholds of a few keV (electron equivalent) are required. The reduced light yield relative to minimum ionizing particles (such as electrons) is described by the scintillation efficiency $\mathcal{L}_{\text{eff}}$ which depends on the recoil energy. Since quenching in LAr is poorly known we are investigating the response to neutrons. For this purpose we have built a neutron scattering facility in our laboratory at CERN (see Fig. 1.1).

Up to $2{\cdot}10^6 \text{s}^{-1}$ 2.45 MeV neutrons from the two-body fusion reaction $dd \rightarrow {}^3\text{He} + n$ are emitted isotropically. The reaction chamber is shielded by a 1.6 t polyester cylinder with 2 mm Pb cladding, keeping an acceptable radiation dose from neutrons and X-rays. The structure of the cryogenic cell is shown in the inset of Fig. 1.1. Scintillation light was detected by two Hamamatsu R6091-01 photomultipliers (PMTs) separated by 47 mm defining a cylindrical sensitive volume of 0.2 ℓ. The inner walls of the cell were lined with Tetratex (Teflon) reflector foil. Both this foil and the PMT windows were coated with tetraphenyl-butadiene (TPB) by vacuum evaporation. TPB shifts the 128 nm wavelength of the VUV scintillation light to the range of maximum sensitivity of the bialkali photocathodes around 420 nm.

Neutrons scattering off the LAr are detected by an organic liquid scintillator at varying angle θ which defines the energy of the recoiling argon nucleus. Pulse shape discrimination allows to distinguish between neutrons and photons. In addition, the neutron time of flight helps to reduce background, mainly from inelastic collisions.

1.1 Pulse shape analysis

Liquid argon generates fast and slow light with decay times of $\tau_1 \simeq 6$ ns (from the excimer singlet state) and $\tau_2 \simeq 1.6$ μs (from the triplet state). Above 10 keV heavily ionizing particles feed mostly the fast component, while electrons contribute mostly to the slow component[1].

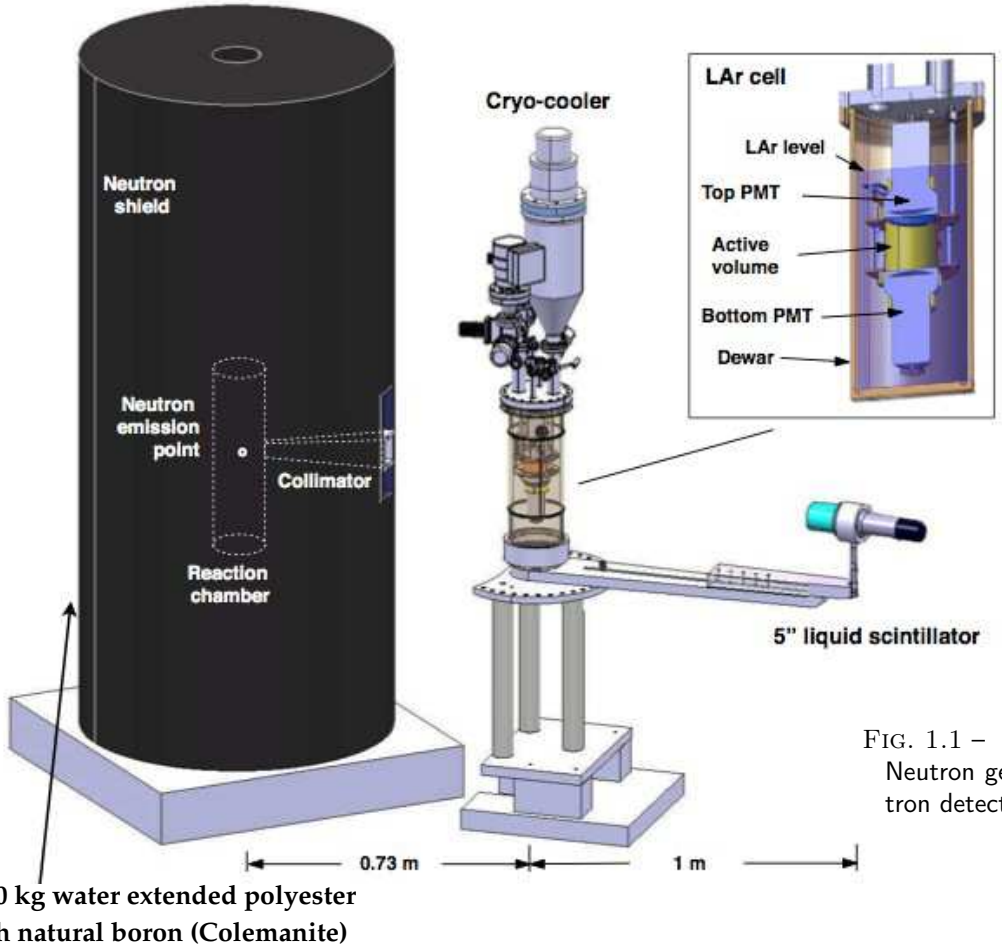

FIG. 1.1 – Neutron generator, LAr target and neutron detector. Inset: LAr target cell.

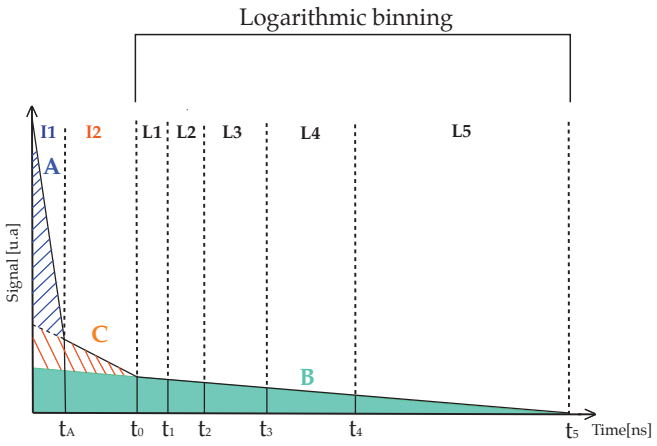

FIG. 1.2 – LAr scintillation signal (logarithmic scale) with the three exponential components A - C, and the time intervals used in the waveform analysis for particle identification (see text).

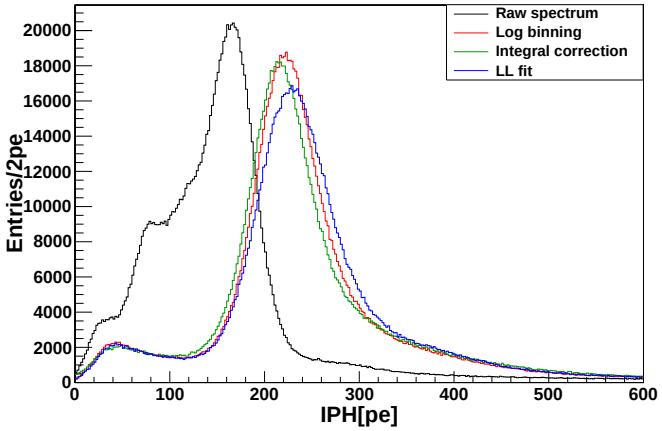

FIG. 1.3 – Distribution of number of photoelectrons (p.e.) observed from a ^{241}Am source (60 keV-γ) combining runs with various LAr purity levels which broadens the energy distribution (black curve). Applying the log binning method (see text) improves the spectrum significantly.

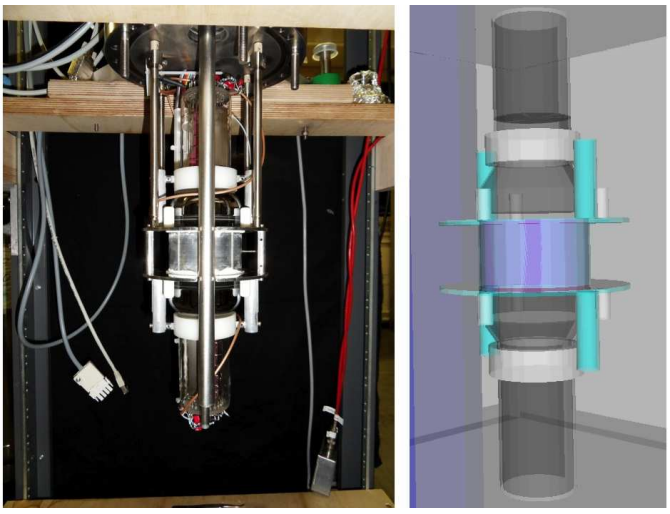

FIG. 1.4 – Picture (left) and GEANT4 model (right) of the LAr cell.

Impurities in LAr (such as N_2, O_2, H_2O and $CO+CO_2$) can absorb VUV scintillation light or quench argon excimer states. The latter process decreases the measured τ_2 and induces losses in the scintillation light (slow part) [2].

In 2012 we developed a method to reconstruct the undisturbed scintillation components from the measured pulse shape. The light pulse is divided in time intervals (Fig.1.2) corresponding to fast (I1) and slow (L) light emission, as well as to a weak intermediate state (I2) [1]. Impurities only affect the late regions of the light pulse so only the slope of slow component B but not its amplitude at t=0. The latter is found most accurately from the weighted mean of the (equal) entries in logarithmically sized integration intervals L1...L5 (spaced according to the *measured* slope of B). Once B is reconstructed, C is found from the I2 integral after subtraction of the contribution from B and, finally, A is found from the I1 integral after subtraction of the contributions from B and C. The total light yield is given by the sum of all components, where the observed B is replaced by the undisturbed distribution (green component in Fig.1.2) based on the measured amplitude at t=0 and the true decay time of 1.6 μs. Details on this technique can be found in [3] and [1].

Figure 1.3 shows light yield spectra of ^{241}Am 60 keV photons from a mix of LAr data samples with varying purity levels. Different pulse shape analysis schemes are compared. The logarithmic binning method described above gives both the best resolution and the smallest systematic error.

1.2 $\mathcal{L}_{\text{eff}}$

A GEANT4 description of the neutron experiment includes the neutron generator with its shielding and collimator, the various components of the LAr detector (cryostat, vessel, reflector foil, PMTs, support frame, etc.) and the liquid scintillators. In Fig.1.4 the simulated LAr cell is compared with the real piece of equipment.

Neutrons of 2.45 MeV were generated isotropically in 4π and 10^8 events were simulated for each scattering angle. In Fig. 1.5 the recoil energy distribution for a scattering angle of 40° is decomposed in various contributions. As can be seen the majority of the events undergo a single scattering in the LAr cell.

A comparison with the measured spectrum shown in Fig. 1.6 enables a determination of the LAr light yield $\mathcal{L}_{\text{eff}}$ for neutron interactions. A χ^2 minimization was performed which uses the energy resolution as a second free parameter. The best fit, illustrated by the red histogram in Fig. 1.6, is obtained for $\mathcal{L}_{\text{eff}} = 0.289 \pm 0.012$.

Finally, we show in Fig. 1.7 and Table 1.1 our results for the light yield $\mathcal{L}_{\text{eff}}$, as a function of scattering angle.

[1] The nature of this component is uncertain. It could be due, for example, to recombining ionisation charge or to collisional triplet to singlet transitions.

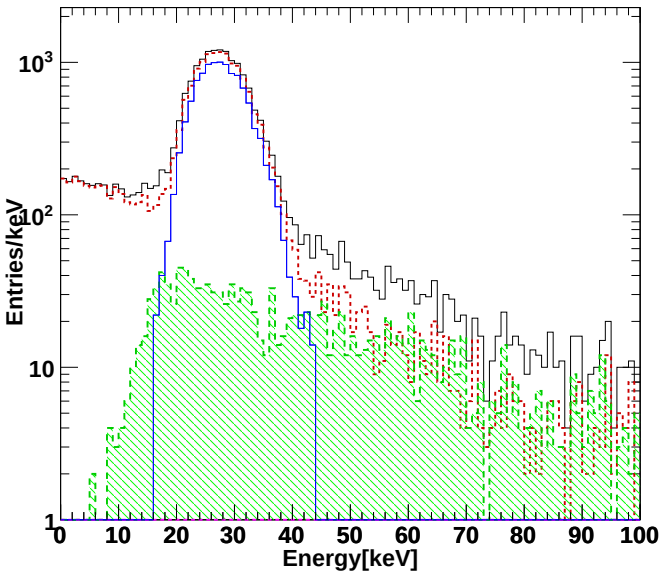

FIG. 1.5 –
Simulated spectrum at $\theta = 40^{o}$ after a time of flight cut at 41 - 48 ns. 58% of the events are contained in a dominant peak (blue) at the 28.5 keV energy deposit expected for a single elastic scattering at this angle. 9.4% of them scatter more than once in the cell resulting in a high-energy tail (green). In 33% of the cases the neutron scatters elsewhere before and/or after the interaction with argon (dashed red). The contribution from inelastic neutron scattering is negligible.

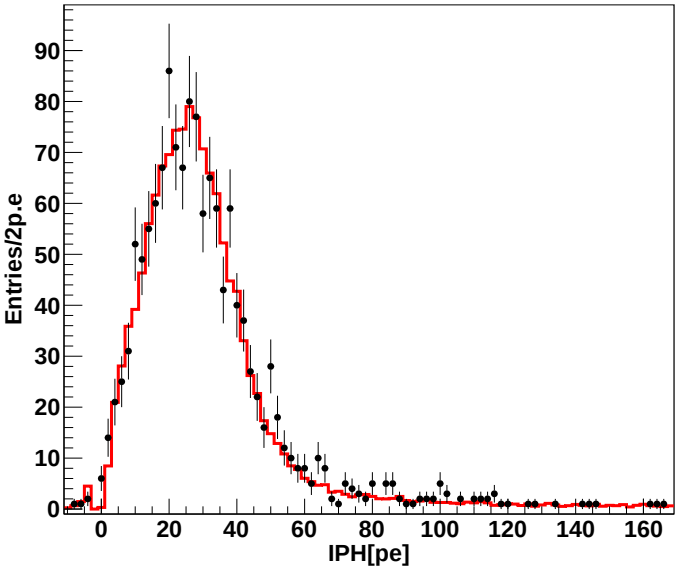

FIG. 1.6 –
Measured pulse height distribution at 40^{o} and best fit of the simulated recoil spectrum (red histogram).

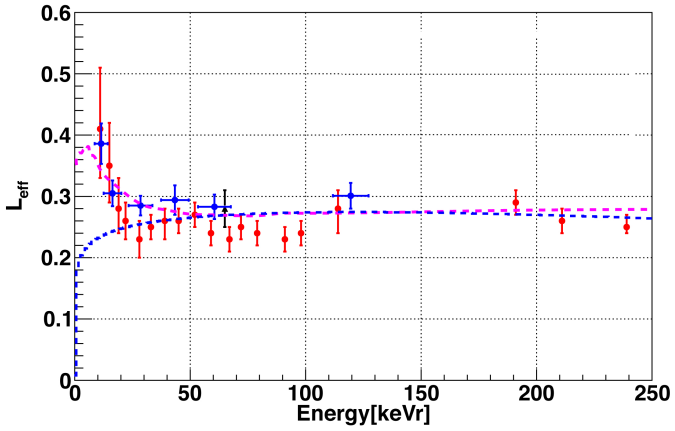

FIG. 1.7 – $\mathcal{L}_{\text{eff}}$ vs. recoil energy. The data points are from this work [3] (blue), from micro-Clean [4] (red) and from WARP [5] (black point at 67 keV). The blue and pink dashed lines are predictions from the Mei [6] and the NEST [7] models, respectively. These values update the preliminary results [1].

TAB. 1.1 –
Results for $\mathcal{L}_{\text{eff}}$ from argon recoils (relative to electrons) vs. scattering angle θ.

θ [°]	Recoil energy [keV]	$\mathcal{L}_{\text{eff}}$
25	11.4	0.386 ± 0.033
30	16.4	0.305 ± 0.021
40	28.5	0.289 ± 0.012
50	43.4	0.294 ± 0.024
60	60.5	0.283 ± 0.020
90	119.5	0.301 ± 0.021

[1] C. Regenfus *et al.*, Journal of Physics: Conference Series **375** (2012) 012019, arXiV:1203.0849.

[2] V. Boccone *et al.*,
J. of Instrumentation **4** (2009) P06001.
C. Amsler et al.,
J. of Instrumentation **5** (2010) P11003.

[3] W. Creus, PhD-thesis, Universität Zürich (submission in June 2013).

[4] D. Gastler *et al.*, Phys. Rev. **C 85** (2012) 065811.

[5] R. Brunetti *et al.*, New Ast. Rev. **49** (2005) 265.

[6] D.–M. Mei *et al.*, Astropart. Phys. **30** (2008)12.

[7] M. Szydagis *et al.*, arXiv: 1106.1613.